

View Article Online
View Journal

# ChemComm

Chemical Communications

### **Accepted Manuscript**

This article can be cited before page numbers have been issued, to do this please use: M. Zhang, L. Cui, Y. Jiang, R. Gao, H. Hao and M. Huang, *Chem. Commun.*, 2025, DOI: 10.1039/D5CC04864H.



This is an Accepted Manuscript, which has been through the Royal Society of Chemistry peer review process and has been accepted for publication.

Accepted Manuscripts are published online shortly after acceptance, before technical editing, formatting and proof reading. Using this free service, authors can make their results available to the community, in citable form, before we publish the edited article. We will replace this Accepted Manuscript with the edited and formatted Advance Article as soon as it is available.

You can find more information about Accepted Manuscripts in the <u>Information for Authors</u>.

Please note that technical editing may introduce minor changes to the text and/or graphics, which may alter content. The journal's standard <u>Terms & Conditions</u> and the <u>Ethical guidelines</u> still apply. In no event shall the Royal Society of Chemistry be held responsible for any errors or omissions in this Accepted Manuscript or any consequences arising from the use of any information it contains.



This article is licensed under a Creative Commons Attribution 3.0 Unported Licence.

Open Access Article. Published on 28 Oktober 2025. Downloaded on 2025-10-29 1:23:23 vm.

### ChemComm

View Article Online DOI: 10.1039/D5CC04864H

### COMMUNICATION

## First-Principles Insights into the Direct Synthesis of Acetic Acid from CH<sub>4</sub> and CO<sub>2</sub> over TM-Si@2D Catalysts

Mingyuan Zhang,<sup>a</sup> Linxia Cui,<sup>a</sup> Yang Jiang,<sup>a</sup> Rui Gao,<sup>a</sup> Haigang Hao<sup>\*a</sup> and Meilan Huang<sup>\*b</sup>

Received 00th January 20xx, Accepted 00th January 20xx

DOI: 10.1039/x0xx00000x

The direct synthesis of acetic acid from natural gases has attracted great attention. However, achieving selective C–C coupling remains a major challenge. We designed doped single-atom transition metal catalysts on 2Ds materials, guided by DFT calculations on the reaction pathways for acetic acid synthesis via CH<sub>4</sub>/CO<sub>2</sub> coupling. Among the catalysts examined, Ni-Si@h-BN shows strong electron synergy in CH<sub>4</sub> activation and C–C coupling under the E–R mechanism, confirmed by kinetics.

Transforming CH<sub>4</sub> and CO<sub>2</sub> into acetic acid offers a green route to convert greenhouse gases into value-added chemicals1. Understanding the reaction mechanism is essential for catalyst design: CH<sub>4</sub> first dissociates into CH<sub>3</sub>\* and H\*, after which CH<sub>3</sub>\* couples with CO₂ to form CH₃COO\*. This intermediate undergoes hydrogenation to yield  $CH_3COOH$ , which subsequently desorbs as acetic acid<sup>2</sup>. Homogeneous catalysts like Pd(OAc)<sub>2</sub>/Cu(OAc)<sub>2</sub>/K<sub>2</sub>S<sub>2</sub>O<sub>8</sub>/CF<sub>3</sub>COOH<sup>3</sup>, RhCl<sub>3</sub><sup>4</sup>and PdSO<sub>4</sub><sup>5</sup> have been used for this conversion but it is challenging to recycle the catalysts. More practical heterogeneous catalysts use supports like TiO<sub>2</sub>, Al<sub>2</sub>O<sub>3</sub>, SiO<sub>2</sub> and zeolites, with active sites such as Zn or Cu<sup>6</sup>. For instance, Cu-K-ZSM-5 zeolite<sup>7</sup> converts CH<sub>4</sub> and CO<sub>2</sub> to acetic acid at 500°C, achieving 5% CH<sub>4</sub> conversion and 100% acetic acid selectivity after 1 hour, while ZnO-CeO<sub>2</sub> supported on montmorillonite<sup>8</sup> achieves 8.33% CH<sub>4</sub> conversion and 100% selectivity at 300°C. Zn-based catalysts generally show higher activity than Cu-based ones but they still require stringent conditions for effective activation9. Theoretical calculations can underpin experimental efforts to improve catalyst activity by revealing reaction pathways and energy barriers. In particular, understanding the elementary steps of C-H activation and subsequent C-C coupling is especially important for the direct synthesis of acetic acid catalysts<sup>10</sup>. Langmuir-Hinshelwood (L-H) and Eley-Rideal (E-R) mechanisms are two commonly adopted mechanisms for CO<sub>2</sub>-CH<sub>3</sub>\* coupling. Nie et al. 11 found that Fe/ZnO₂ catalysts activate CH<sub>4</sub> efficiently due to Fe-Zn bimetallic synergy, with low barriers for CH<sub>4</sub> activation (0.30 eV) and C-C bond formation (0.75 eV) via the L-H pathway. However, the L-H mechanism requires dual adsorption sites, which increases the probability of side reactions<sup>12</sup>. The E-R mechanism, involving reactions between gas-phase molecules and adsorbed species, usually reflects experimental conditions<sup>13</sup>. When CH<sub>4</sub> and CO<sub>2</sub> compete for adsorption sites, the relative adsorption strengths govern which pathway becomes dominant. In Zn-ZSM-5 catalysts14, CH<sub>4</sub> preferentially adsorbs on Zn<sup>2+</sup> sites to form CH<sub>3</sub>\* intermediates, while CO<sub>2</sub> shows weak affinity (<0.2 eV), thus gas-phase CO<sub>2</sub> couples directly with adsorbed CH<sub>3</sub> following an E-R mechanism. Although Zn-ZSM-5 lowers the barriers for CH<sub>4</sub> activation (0.65 eV) and acetate formation (0.20 eV), its C-C coupling activity remains limited (1.79 eV), underscoring the need to exploit selective C-C bond formation by other transition metal catalysts under E-R pathway. Catalysts with well-defined single-site active units15—such as isolated metal atoms with specific coordination environments or tailored metal-support interfaces—are highly promising for enhancing C–C coupling via the E-R mechanism.

Nickel is commonly used for CH<sub>4</sub> conversion due to its high activity, but it is prone to coking and sintering<sup>16</sup>. Studies show that adding Si atoms in Ni-Si/ZrO2 catalysts enhances Ni dispersion, stability, and resistance to coking during CH₄ and CO<sub>2</sub> dry reforming<sup>17</sup>. This inspired us to examine the effect of Si on the electron density of Ni-based catalysts, to optimize Ni sites for coupling CH4 and CO2 into acetic acid. On the other hand, single-atom catalysts (SACs) on 2D materials have shown significant potential for CO<sub>2</sub> conversion, owing to their high atom utilization and activity, for example, Feng et al. demonstrated that SACs embedded in 2D graphitic carbon nitride support exhibit high catalytic efficiency<sup>18</sup>. For example, Zn-based metal oxide SACs show unique catalytic properties for converting CH<sub>4</sub> and CO<sub>2</sub> to acetic acid; however, efficient C-C coupling remains a challenge19. The high surface area and stability of two-dimensional (2D) materials enable SACs@2D systems with well-defined active centres, surpassing conventional metal oxide supports<sup>20</sup> and potentially improving C-C coupling. Herein, we designed SACs composed of transition metals (Mn, Fe, Co, and Ni) doped with Si promoters on h-BN

<sup>&</sup>lt;sup>a</sup> School of Chemistry and Chemical Engineering, Inner Mongolia University, Hohhot, Inner Mongolia 010021, China. E-mail: haohaigang@imu.edu.cn.

b. School of Chemistry and Chemical Engineering, Queen's University, Belfast, BT9 5AG, UK. E-mail: m.huang@qub.ac.uk

C Supplementary Information available: [details of any supplementary information available should be included here]. See DOI: 10.1039/x0xx00000x

This article is licensed under a Creative Commons Attribution 3.0 Unported Licence.

Open Access Article. Published on 28 Oktober 2025. Downloaded on 2025-10-29 1:23:23 vm..

**COMMUNICATION** ChemComm

(TM-Si@h-BN) to identify optimal active component. Subsequently, we evaluated various 2D materials, including graphene (GR), N<sub>4</sub>-doped graphene (N<sub>4</sub>@GR), and phosphorene (P), to determine the optimal catalyst configuration. We demonstrated that Ni-Si@h-BN is a promising alternative to traditional catalysts and elucidated its activation and reaction mechanism: electron transfer from Si to Ni creates an electronrich Ni site (Ni<sup>-2.16</sup>) and its moderate work function is favourable for electron balance, facilitating CH<sub>4</sub> activation and CO<sub>2</sub> adsorption.

The computed binding energy ( $E_b$ ) and formation energy ( $E_f$ ) <sup>21</sup> for TM-Si@h-BN catalysts demonstrate the stability of Si and TM atoms on h-BN (Table S1). AIMD simulations of the TM-Si@h-BN catalysts structure at 500 K demonstrate its thermodynamic stability (Fig. S1a, b). Bader charge calculations (Table S1) show electrons transfer from Si to transition metals, forming a  $TM_1^{\delta^-}$ -Si<sub>1</sub><sup> $\delta^+$ </sup> distribution. We compared the adsorption abilities of CH<sub>4</sub> and CO<sub>2</sub> at 500 K. Although both CH<sub>4</sub> and CO<sub>2</sub> exhibit relatively weak interactions with the surfaces, CH<sub>4</sub> binds more strongly (-0.36  $\sim$  0.15 eV) than CO<sub>2</sub> (0.22  $\sim$  0.65 eV) on all TM-Si@h-BN catalysts, underscoring that CH<sub>4</sub> is preferentially activated across these materials (Fig. S1c, d). The work function (Fig. S2), reflecting the electron transfer ability of TM-Si@h-BN, controls CH<sub>4</sub> and CO<sub>2</sub> adsorption such that CH<sub>4</sub> adsorption weakens with increasing work function, while  $CO_2$  adsorption strengthens (Fig. S3a).

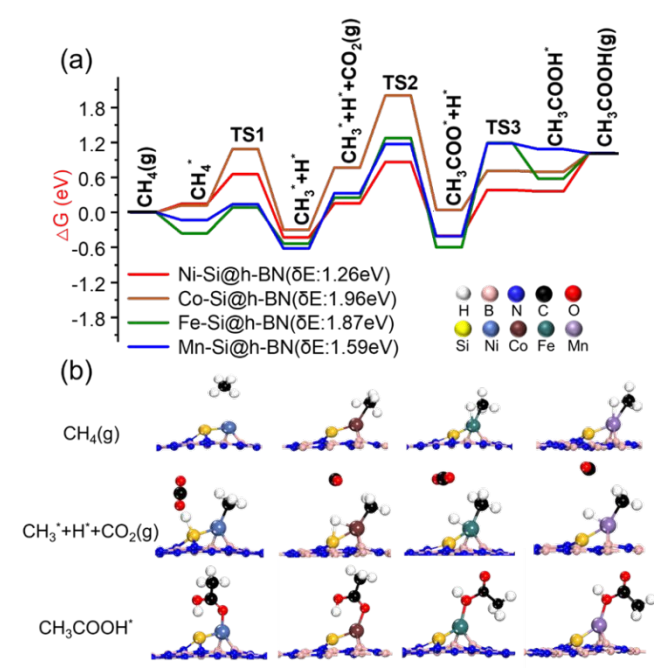


Fig 1. The coupling of CH<sub>4</sub> and CO<sub>2</sub> into acetic acid on TM-Si@h-BN at 500 K. (a) Reaction energy profile (energy span, δE is shown in parentheses). (b) Adsorption configurations of key reactants and products. See Fig. S6 and Table S4 for details.

The dissociation of CH<sub>3</sub>\* at TM sites is influenced by the presence of doped Si. On Mn-Si@h-BN and Fe-Si@h-BN, the H atom is co-adsorbed with  ${\rm CH_3}^*$  on the top site of TM, exhibiting low energy barriers of 0.27 and 0.44 eV (Fig. 1 and Table S4),

respectively. On Co-Si@h-BN, H\* prefers the Co-Si\_bridge\_site. with a higher barrier of 0.96 eV. On Ni-Si@hlBN,3the5figdA8geh atom migrates to the top site of Si, incurring an energy barrier of 0.50 eV. The C-C coupling is initiated by the reaction of CH<sub>3</sub>\* and gaseous CO<sub>2</sub>, forming the CH<sub>3</sub>COO\* intermediate at TM sites via the E-R mechanism. Ni-Si@h-BN shows the lowest barrier for this step (0.71 eV) among the TM-Si@h-BN catalysts, and crystal Hamilton population (COHP) analysis reveals a weaker Ni-CH<sub>3</sub> bond (integrated strength ICOHP: -1.18 eV) that facilitates CO2 insertion (Fig. S7). The hydrogenation of CH<sub>3</sub>COO\* to acetic acid generally proceeds with high barriers on TM-Si@h-BN. Furthermore, the energetic span model ( $\delta E$ ) was employed as a direct descriptor of the catalytic cycle rate<sup>22</sup>. At 500 K, except for Mn–Si, where TS3 (CH<sub>3</sub>COO\* hydrogenation) is the turnover-determining transition state (TDTS), TS2 (C-C coupling) serve as the TDTS for the other TM-Si systems exhibit, while CH<sub>3</sub>COO\* + H\* act as the turnover-determining intermediate (TDI) in all cases. The corresponding  $\delta E$  values for each system are summarized in Table S12. Notably, Ni-Si@h-BN shows the lowest δE (1.26 eV), emphasizing its superior activity and highlighting its potential as a 2D support for further optimization.

The structural stability of Ni-Si@2D and the thermodynamic stability of Ni-Si@2D at 500 K are confirmed (Fig. S8). Bader charge analysis reveals that silicon donates electrons to transition metals on both Ni-Si@2D and TM-Si@h-BN catalysts, highlighting its general role as an electron donor (Table. S5), and accounting for the stronger CH4 adsorption observed on TM-Si@2D compared to TM@2D (Table S7).

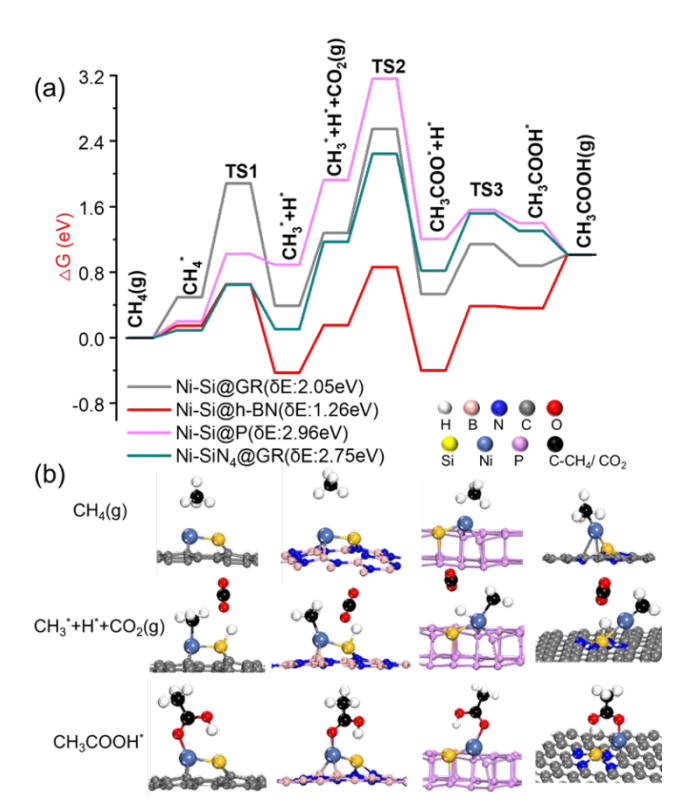


Fig 2. The coupling of CH<sub>4</sub> and CO<sub>2</sub> into acetic acid on Ni-Si@2D at 500 K. (a) Reaction energy profile (energy span, δE is shown

This article is licensed under a Creative Commons Attribution 3.0 Unported Licence.

Open Access Article. Published on 28 Oktober 2025. Downloaded on 2025-10-29 1:23:23 vm..

in parentheses). (b) Adsorption configurations of key reactants and products. See Fig. S9 and Table S9 for details.

The CH<sub>4</sub> adsorption energy on Ni-Si@2D strengthens with increasing work function, whereas the CO<sub>2</sub> adsorption energy exhibits a volcano-shaped trend (Fig. S3b). The Ni atom in Ni-Si@2D were identified as the primary activation site for CH4 dissociation (Fig. 2 and Table S9), with Ni-Si@h-BN exhibiting the lowest barrier (0.50 eV), outperforming Ni-Si@GR, Ni-Si@P, and Ni-SiN<sub>4</sub>@GR. The Bader charge analysis of C-C coupling step (Table S10) reveals that electron transfer from the CH<sub>3</sub>-TM bond to CO<sub>2</sub>, facilitating C-C bond formation. Ni-Si@h-BN exhibits a barrier of 0.71 eV for C-C coupling, which is comparable to other Ni-Si@2D systems and lower than reported E-R pathway catalysts<sup>19.</sup> During acetic acid formation and desorption, most hydrogenation reactions proceed easily on Ni-Si@2D. For Ni-Si@2D catalysts at 500 K, the energy span is smallest on h-BN (1.26 eV), indicating its superior activity. While TS2 (C-C coupling) is the TDTS across all systems, the TDI differs: it is CH<sub>3</sub>COO\* + H\* on Ni-Si@h-BN whereas it is adsorbed CH<sub>4</sub>\* on the others. Together with fast CH4 dissociation, facile C-C coupling, and favourable hydrogenation, Ni-Si@h-BN exhibits markedly enhanced activity compared with other reported catalysts (Table S11). By-product formation during acetic acid synthesis on Ni-Si@h-BN was also evaluated. Energetic span analysis shows that the C–C coupling pathway to  $CH_3COO^*$  ( $\delta E =$ 0.71 eV) is much more favorable than CO₂ hydrogenation routes via COOH or HCOO ( $\delta E = 1.97$  and 0.81 eV), indicating C-C coupling dominates over formic acid formation (Fig. S12).

To further understand temperature effects, the energetic spane was analysed at different temperatures, and the corresponding TDTS and TDI are summarized in Table S12. Ni–Si@h-BN exhibits the lowest  $\delta E$  across 300–900 K, reaching 1.23 eV at 600 K (Fig. S13). Based on the energetic span model, TOFs for acetic acid formation (300–900 K, 1 bar) <sup>23</sup> were calculated (Fig. 3), showing consistently highest TOFs for Ni–Si@h-BN, with a peak at 700 K (8.02 ×  $10^{-2}$  s<sup>-1</sup>, logTOF: 2.90), after which TOFs decreases with further temperature increase. These results highlight Ni–Si@h-BN as an efficient catalyst for CH<sub>4</sub> and CO<sub>2</sub> conversion under moderate conditions while minimizing coke formation<sup>24</sup>.

COMMUNICATION

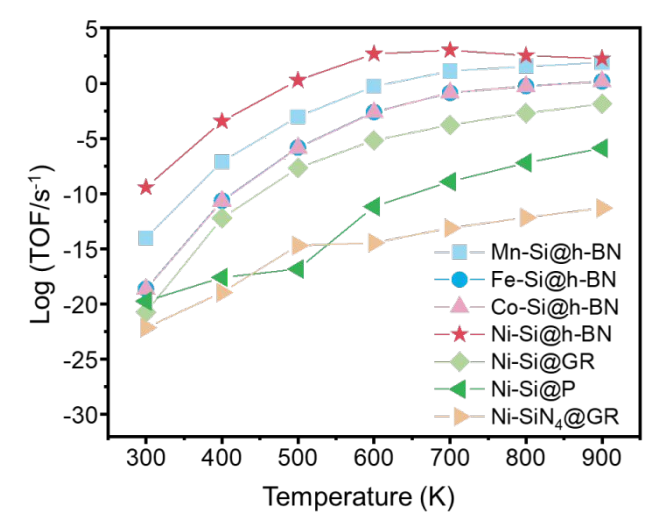


Fig. 3 Turnover frequencies for CH₃COOH production over TM—Si@2D as a function of temperature (CH₄/CO₂ = 1:1, 1 bar).

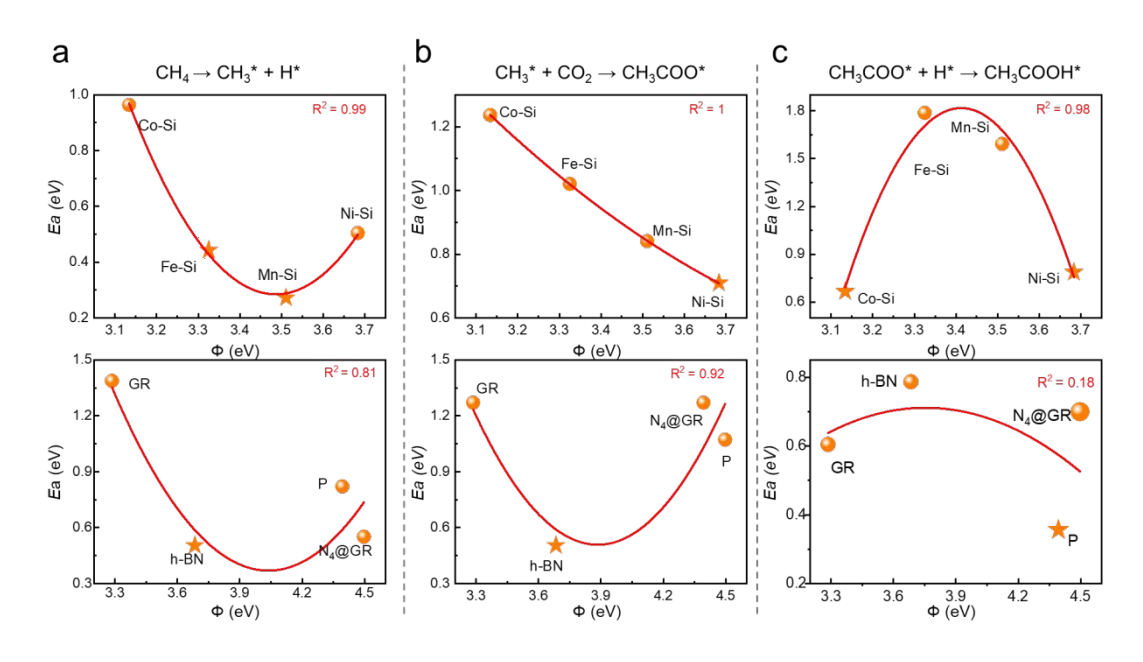


Fig. 4 Relationship between work function (φ) and energy barriers (Ea) for acetic acid synthesis from CH₄ and CO₂ on TM-Si@2D at 500 K: (a) CH₄ dissociation; (b) C−C coupling; (c) acetic acid formation. Upper panel: the 2D material is h-BN, Lower panel: The transition metal is Ni-Si on different 2D materials.

Understanding the relationship between catalytic performance and electronic properties is crucial for designing new catalysts for efficient CH<sub>4</sub>–CO<sub>2</sub> coupling toward acetic acid. CH<sub>4</sub>

dehydrogenation on TM–Si@2D exhibits a volcano dependence on work function (Fig. 4a), with the lowest barriers with moderate values (3.3–4.0 eV) due to optimal polarization of the

COMMUNICATION ChemComm

C–H bond. For C–C coupling (Fig. 4b), most TM–Si@2D follow a volcano-like behaviour, whereas TM–Si@h-BN shows a nearly linear decrease in barrier with increasing work function, benefiting from  $\pi$  back-donation that enhances CO2 adsorption and facilitates CH3\* activation. In contrast, CH3COO hydrogenation follows an inverse volcano relationship to the work function (Fig. 4c), showing reduced barriers at both low and high work function values. Bader charge analysis (Fig. S14) further confirms that higher TM electron density generally is attributed to reduced barriers throughout entire reaction process. Ni-Si@h-BN, characterized by an electron-rich Ni site (Ni-2.16) and a moderate work function (3.68 eV), exhibits the lowest barrier in the rate-determining step and thus maintains thermodynamic favourability across all three elementary steps. This results from its balanced electron donation to the substrate with optimal adsorption strength.

We elucidated the acetic acid synthesis mechanism from  $CO_2$  and  $CH_4$  and designed TM-Si@2D based on DFT calculations. Silicon incorporation enriches transition metals with electrons, generating electron-rich active sites that enhance the catalytic activity. Ni–Si@h-BN stands out among doped transition metal catalysts. Its moderate work function and high Ni electron density facilitate  $CH_4$  activation, while the  $Ni_1^{\delta^-}$ – $Si_1^{\delta^+}$  synergy enables C–C coupling through the E–R mechanism. The turnover frequency for  $CH_4$  and  $CO_2$  conversion to acetic acid reaches  $8.02 \times 10^{-2} \, \text{s}^{-1}$  at 700 K and 1 bar, demonstrating the reaction's feasibility under practical conditions. This advantageous electronic structure underpins its capability for efficient and selective acetic acid synthesis.

This study was supported by the National Natural Science Foundation of China (No.22172083, 22462020), the 111 Project (D20033). We also acknowledge Inner Mongolia China HPC Technology Co. LTD and Kelvin2 from NI-HPC at Queen's University Belfast for its Super-Server for the DFT calculations.

#### Conflicts of interest

There are no conflicts to declare.

### **Data availability**

The data supporting this article have been included as part of the Supplementary Information.

### **Notes and references**

- (a) Y. Li, K. Zheng, Y. Shen, M. Huang, B. Liu, Y. Xu and X. Liu, J. Phys. Chem. C, 2023, 127, 5841–5854;(b) B.-S. Mu, Y. Zhang, M. Peng, Z. Tu, Z. Guo, S. Shen, Y. Xu, W. Liang, X. Wang, M. Wang, D. Ma, Z. Liu, Angew. Chem. Int. Ed., 2024, 63, e202407443.
- 2 X. Zan, S. Tao, C. Zhang, Y. Wu, Y. Liu and W. Huang, J. Energy Inst. 2024, 116, 101739
- 3 Fujiwara, Y., Taniguchi, Y. and Takaki, K, Stud. Surf. Sci. Catal., 1997, 107, 275–278.
- 4 Hristov, I. H. and Ziegler, T., Organometallics 2003, 22, 3513–3525.

- 5 Chempath, S. and Bell, A. T., J. Am. Chem. Soc. 2006, 128, 4650–4657.
  DOI: 10.1039/D5C.C04864H
- (a) Riguang Z and Wei H, B. W., Chinese J. Catal. 2008, 29, 913;
   (b) Liu, Y., Cui, N., Jia, P. and Huang, W., Catalysts 2020, 10, 131;
   (c) Shahzad, N.; Khan, B., J. Mol. Graph. Model. 2021, 105, 107896.
- 7 Rabie, A. M.; Betiha, M. A. and Park, S. E. Appl. Catal. B Environ. 2017, 215, 50–59.
- 8 Shavi, R.; Ko, J.; Cho, A. and Han, J. W., *Appl. Catal. B Environ.* 2018, 229, 237–248.
- (a) Chen J., Xu W., and Zhang H., ACS Appl. Nano Mate., 2024,
   7, 11285-11294.; (b) Liu N., Lu N., and Zhao K., Chem. Eng. J.,
   2024, 487: 150690.
- 10 Tu C., Nie X. and Chen J. G., ACS Catal. 2021, 11, 3472-3482.
- 11 Nie X., Ren X. and Tu C., Chem. Commun., 2020, 56, 3983-3986.
- (a) Liu C., Li X. and Wang Y., ChemCatChem, 2016, 8, 421–433.;
  (b) Hu B., Yang H., and Luo Y., J. Catal., 2019, 369, 331–343.;
  (c) Wu H, Singh-Morgan A, and Qi K, ACS catal., 2023, 13: 5375-5396.;
  (d) Zhu L, Lin Y, and Liu K, Chin. J. Catal., 2021, 42: 1500-1508.
- 13 (a) Y. Wang, G. Wu, M. Yang, and J. Wang, J. Phys. Chem. C, 2013, 117: 8767-8773; (b) D. Kiani and I. E. Wachs, ACS Catal., 2024, 14: 16770–16784.
- 14 Mahyuddin M H, Tanaka S, and Shiota Y, *Bull. Chem. Soc. Jpn.*, 2020. 93: 345-354.
- (a) D. Kiani and I. E. Wachs, ACS Catal., 2024, 14, 16770–16784.;
   (b) Wang J., Song Q., Shang Y., Liu Y. and Zhao J., Nanomaterials, 2023, 15, 1111.
- (a) Benrabaa R. Löfberg A. and Rubbens A., Catal. Today, 2013, 203, 188–195; (b) Niu J., Ran J. and Chen D., Appl. Surf. Sci. 2020, 513, 145840; (c) Li J., Croiset E., and Ricardez-Sandoval L., Appl. Surf. Sci. 2014, 311, 435–442.
- 17 Wang Y., Yao L., and Wang Y., *ACS catal.* 2018, 8, 6495–6506; Li L., Wang Y., Zhao Q., *Catalysts* 2021, 11, 1–14.
- (a) Feng J., Gao H. and Zheng L., Nat. Commun. 2020, 11, 1–8;
   (b) Yuan J., Zhang W., and Li X., Chem. Commun. 2018, 54, 2284–2287.;
   (c) Homlamai K., Maihom T., and Choomwattana S., Appl. Surf. Sci. 2020, 499, 143928.
- 19 (a) Zhang P, Yang X, and Hou X, Catal. Sci. Technol., 2019, 9: 6297-6307; (b) Li R, Wu J, and Zhao X, Chem. Eng. J., 2024, 490: 151528.
- 20 (a) Zamalloa-Serrano J M, Mendieta-Moreno J I, and Gómez-Fernández J M, Carbon, 2024, 229: 119544; (b) Cheng Y, Zhou J., Iscience, 2024, 27: 108788.
- 21 Cui L., Shi K. and Zhang M. Fuel, 2023, 340: 127541.
- 22 (a) Kozuch, S., Shaik, S. Acc. Chem. Res. 2011, 44: 101–110; (b) Chen, J., Chen, Y., Li, P., Wen, Z., and Chen, S., ACS Catal., 2018, 8: 10590-10598.
- (a) Y. Zhao, H. Wang, J. Han, X. Zhu, D. Mei and Q. Ge, ACS Catal., 2019, 9: 3187–3197; (b) A. M. Rabie, M. M. Hassan, E. A. El-Sharkawy and A. E. Awadallah, Appl. Catal. B-Environ., 2017, 215: 50–59; (c) M. G. Sibi, S. Chandran, R. C. Devarajan and N. R. Shiju, ACS Catal., 2021, 11: 8382–8398.
- 24 (a) L. He, M. Li, W.-C. Li, W. Xu, Y. Wang, Y.-B. Wang, W. Shen and A.-H. Lu, ACS Catal., 2021, 11: 12409–12416; (b) J. W. Han, C. Kim, J. S. Park and H. Lee, ChemSusChem, 2014, 7: 451-456.

View Article Online DOI: 10.1039/D5CC04864H

The data supporting this article have been included as part of the Supplementary Information.